Molecular Therapy
Nucleic Acids
Original Article

MicroRNA-142a-3p regulates neurogenic skeletal muscle atrophy by targeting Mef2a

Xinyi Gu,[1,2,4] Shen Wang,[1,2,4] Dongdong Li,[1,2] Bo Jin,[1,2] Zhidan Qi,[1,2] Jin Deng,[1,2] Chen Huang,[1,2] and Xiaofeng Yin[1,2,3]

[1]Department of Orthopedics and Traumatology, Peking University People's Hospital, Beijing, China; [2]Key Laboratory of Trauma and Neural Regeneration (Peking University), Beijing, China; [3]Pizhou people's Hospital, Pizhou, China

Peripheral nerve injury can lead to progressive muscle atrophy and poor motor function recovery, which is a difficult point of treatment, and the mechanism needs to be further explored. In previous studies, we found that miR-142a-3p was significantly upregulated and persistently highly expressed in denervated mouse skeletal muscle. Here, we show that overexpression of miR-142a-3p inhibited the growth and differentiation of C2C12 myoblast, while knockdown of miR-142a-3p had a promoting effect. *In vitro*, knockdown of miR-142a-3p in denervated mouse skeletal muscle effectively increased proliferating muscle satellite cells and ameliorated muscle atrophy. Mechanistically, the myoregulator Mef2a was proved to be an important downstream target of miR-142a-3p, and miR-142a-3p regulates skeletal muscle differentiation and regeneration by inhibiting the expression of Mef2a. The co-knockdown of Mef2a and miR-142a-3p effectively alleviated or offset the biological effects of miR-142a-3p knockdown. In conclusion, our data revealed that miR-142a-3p regulates neurogenic skeletal muscle atrophy by targeting Mef2a.

INTRODUCTION

Muscle atrophy is a major cause of motor function loss after peripheral nerve injury (PNI). At present, the treatment of PNI mainly focuses on restoring the continuity of the nerve, while ignoring the protection of the distal effector. Clinically, most patients with nerve injury will have different degrees of muscle atrophy after surgery.[1,2] Therefore, attention should be paid to the prevention and treatment of skeletal muscle atrophy after PNI. And the premise is to fully understand the pathological process and mechanism of denervated skeletal muscle atrophy.

In skeletal muscle, microRNAs have been shown to regulate the fate of myogenic progenitor cells and the dynamic balance of muscle tissue.[3,4] Previously, We conducted full transcriptome sequencing on the gastrocnemius muscle of mice after sciatic nerve injury and found that miR-142a-3p was significantly upregulated and persistently highly expressed in denervated mouse skeletal muscle.[5] Studies have found elevated miR-142-3p levels in mice with Duchenne muscular dystrophy as well as other inherited muscular dystrophies.[6,7]And miR-142a-3p can effectively regulate ion channel currents, which may regulate physiological functions of skeletal muscle.[8] Other studies have found that miR-142-3p has a regulatory effect on muscle energy metabolism. For example, miR-142-3p was found to inhibit lipid utilization in skeletal muscle, complementing miR-27a-3p in regulating muscle fiber metabolism.[9] Overexpression of miR-142a-3p can enhance myocardial mitochondrial function.[10] Based on the above, we believe that miR-142a-3p may play an important role in the process of denervated muscle atrophy.

We used three tools including MR-microT (www.microrna.gr/microT),TarBase v.8, and miRWalk (http://mirwalk.umm.uni-heidelberg.de/) to predict the target genes of miR-142a-3p and then took the intersection. The results showed that miR-142a-3p has a high possibility of binding to Mef2a. Mef2a was also significantly differentially expressed in our sequencing results.[5] And in our past published studies, we obtained the key protein-protein interaction (PPI) network for denervated muscle atrophy by meta-analysis,[11] and by labeling the target genes of miR-142a-3p in this network, we found that Mef2a was one of the target genes closest to the center of the PPI network (Figure S1). Furthermore, Mef2a and its predictive interaction genes (http://genemania.org/) were found to be prominent in the PPI network (Figure S2). That may suggest that Mef2a plays an important role in the pathological process of denervation muscular atrophy. The Mef2 family (Mef2a, -b, -c, and -d) is a class of conserved and highly expressed transcription factors that mainly regulate the expression of muscle-related genes. Mef2 cooperates with members of the MyoD family to activate gene expression and transform fibroblasts into myoblasts.[12,13] However, whether Mef2a has a regulatory function in impaired skeletal muscle remains unknown.

In summary, in this study, we confirmed the targeting relationship between miR-142a-3p and Mef2a through dual luciferase experiments and verified that miR-142a-3p regulates C2C12 proliferation and differentiation by targeting Mef2a. Furthermore, we co-knocked down

Received 7 January 2023; accepted 31 May 2023;
https://doi.org/10.1016/j.omtn.2023.05.023.

[4]These authors contributed equally

Correspondence: Xiaofeng Yin, Department of Orthopedics and Traumatology, Peking University People's Hospital, Beijing, China.
E-mail: xiaofengyin@bjmu.edu.cn

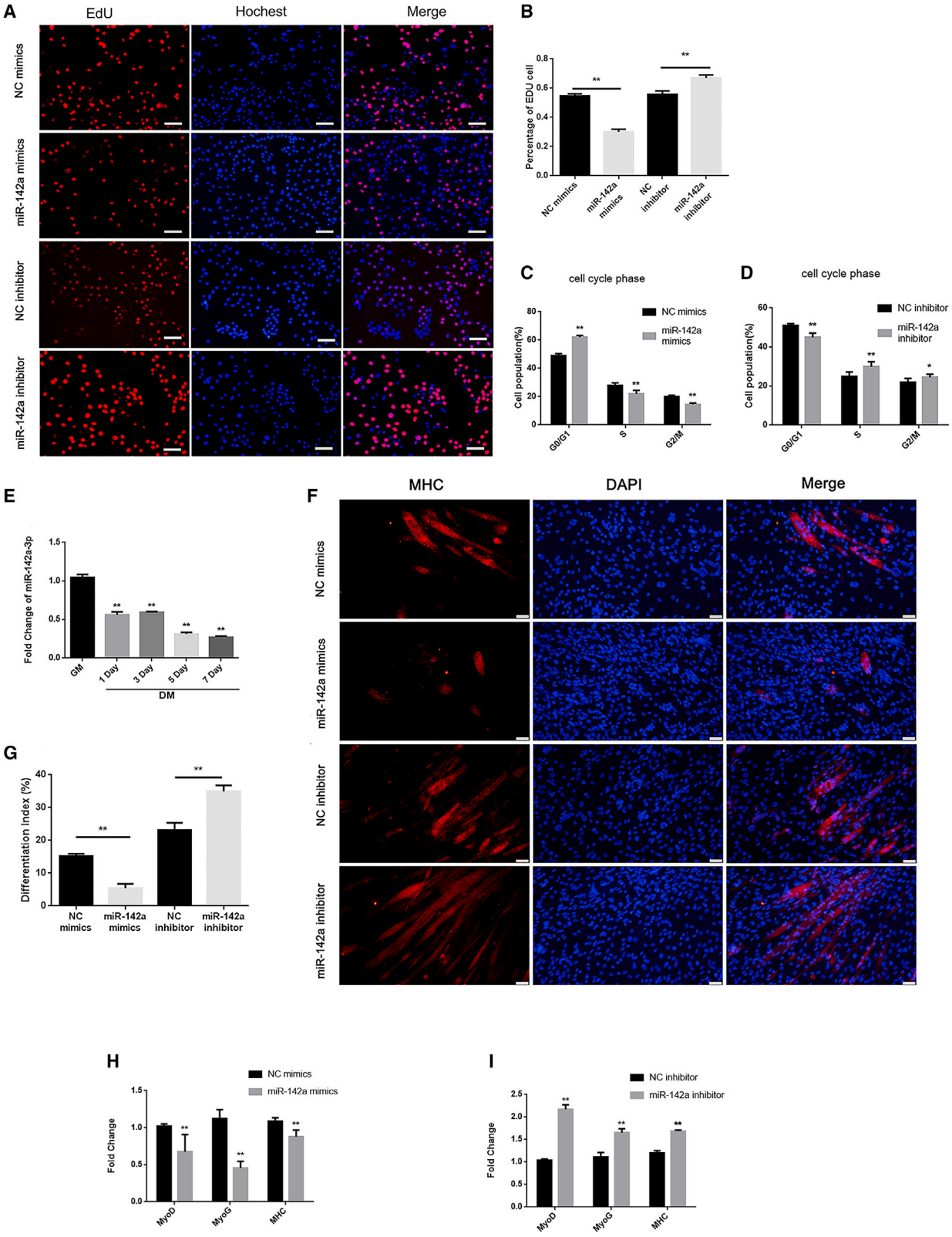

(legend on next page)

miR-142a-3p and Mef2a in mouse skeletal muscle and found that the miR-142a-3p/Mef2a axis has an important regulatory effect on denervated muscle atrophy. These data suggest that inhibition of miR-142a-3p may represent a novel approach for the treatment of neuromuscular atrophy.

RESULTS

miR-142a-3p inhibits the proliferation and differentiation of C2C12 cells

We successfully overexpressed/knocked down miR-142a-3p in C2C12, where only cells with a transfection rate of more than 80% were used in subsequent experiments (Figure S3). Ethidium bromide (EdU) staining showed that the ratio of EdU-positive cells in the miR-142a-3p overexpression group was significantly reduced, while it increased in the miR-142a-3p knockdown group (Figures 1A and 1B) (Table S1). The flow cytometry results showed that the proportion of cells in the G2/M phase was significantly decreased in the miR-142a-3p overexpression group (Figure 1C), and the miR-142a-3p knockdown group had the opposite trend (Figure 1D). The cells of each group were cultured at an equal density, and the expression of miR-142a-3p was detected by qRT-PCR at 0, 1, 3, 5, and 7 days of differentiation. As differentiation progressed, miR-142a-3p expression gradually decreased (Figure 1E). miR-142a-3p overexpression reduced the number of myotubes on the fifth day of differentiation, and miR-142a-3p knockdown increased the number of myotubes (Figures 1F and 1G) (Table S1). The expression levels of MyoD, MyoG, and myosin heavy chain (MHC) in 5-day-differentiated cells were detected. Overexpression of miR-142a-3p inhibited the expression of MyoD, MyoG, and MHC, while the knockdown of miR-142a-3p had the opposite effect (Figures 1H and 1I). In summary, miR-142a-3p can inhibit the differentiation of C2C12 cells.

Mef2a is target gene of miR-142a-3p

According to MR-microT (www.microrna.gr/microT), miR-142a-3p was found to bind to the 3′ UTR of Mef2a (Figure 2A). The 3′ UTR of the target gene Mef2a was constructed behind the reporter gene luciferase in the vector. The inhibitory effect of miRNA on the target gene was quantitatively reflected by comparing the changes of luciferase activity after overexpression of miR-142a-3p. The results of dual luciferase reporter gene detection showed that the relative luciferase activity was reduced when miR-142a-3p and pmirGLO-Mef2a-3′ UTR were cotransfected into HEK-293T cells. However, the mutant pmirGLO-Mef2a-3′ UTR and the empty plasmid control pmirGLO did not change the relative luciferase activity (Figure 2B). These results indicate that Mef2a is the direct target gene of miR-142a-3p. miR-142a-3p overexpression significantly decreased the transcript level and protein expression level of Mef2a in C2C12 cells (Figures 2C–2E). As predicted by TransmiR v2.0 (http://www.cuilab.cn/transmir), the highly conserved MEF2 family proteins, as transcription factors, have binding sites in the promoter region of miR-142a-3p (Figure 2F). 12 pairs of primers were designed in the promoter region of miR-142 (Figure 2G). qRT-PCR was used to detect the expression level of miR-142a-3p in the Mef2a knockdown group and the control group, and it was found that Mef2a knockdown reduced miR-142a-3p expression (Figure 2H). The chip analysis showed that Mef2a did not bind to the miR-142 promoter region (Figure 2I).

miR-142a-3p inhibits C2C12 proliferation and differentiation by targeting Mef2a

We used shRNA-A, -B, -C, and -D to knock down Mef2a in C2C12 cells, and western blot results showed that the knockdown efficiency of shRNA-D was the highest (Figures 3A and 3B). ShRNA-D was used to establish a Mef2a knockdown model, and cells were divided into five groups: the virus-free control group, miR-142 control + Mef2a control group, miR-142 knockdown + Mef2a control group, miR-142 control + Mef2a knockdown group, and miR-142 knockdown + Mef2a knockdown group. An EdU staining experiment was used to compare the proliferation ability of each group of cells (Figures 3C and 3D) (Table S2). Cells of each group were differentiated at the same density for 5 days, and the differentiation index was assessed (Figures 3E and 3F) (Table S2). Next, the gene expression levels of MyoG, MyoD, and MHC were measured (Figures 3G–3I). In contrast to the knockdown of miR-142a-3p, the knockdown of Mef2a inhibited the proliferation and differentiation of C2C12 cells. Co-knockdown of the two showed that Mef2a knockdown reduced the promotion of cell proliferation and differentiation by knocking down miR-142a-3p.

Establishment of animal model

The miR-142a-3p knockdown plasmid and the Mef2a knockdown plasmid were packaged with adeno-associated virus (AAV) to intramuscularly inject the right hind limbs of mice. 1 week after injection, the expression level of AAV label green fluorescent protein (GFP) was observed under a fluorescence microscope (Figure 4A). qRT-PCR and western blotting were used to detect the knockdown efficiency of miR-142a-3p and Mef2a. The knockdown rate of both reached more than 70% (Figures 4B–4D). The mice were divided into five groups: the PBS group, miR-142 control + Mef2a control group, miR-142 knockdown + Mef2a control group, miR-142

Figure 1. MiR-142a-3p inhibits the proliferation and differentiation of C2C12 cells

(A and B) EdU staining results showed that miR-142a-3p reduces the proportion of EdU-positive cells. (C and D) The flow cytometry results showed that miR-142a-3p overexpression blocked more cells in the G0/G1 phase. (E) qRT-PCR showed that miR-142a-3p expression gradually decreased during C2C12 cell differentiation. (F) Immunofluorescence staining: muscle bundles were stained red with an anti-MHC antibody, and cell nuclei were stained blue with DAPI. (G) The differentiation index was assessed as the ratio of MHC-positive cells to the total number of nuclei, and the differentiation index per field showed that miR-142a-3p overexpression inhibited myotube formation. (H and I) MiR-142a-3p overexpression inhibited the mRNA expression of MyoD, MyoG, and MHC (n = 3 per group; scale bar, 500 μm for A and 50 μm for F). NC mimics, overexpression control group; MiR-142a mimics, miR-142a-3p overexpression group; NC inhibitor, knockdown control group; MiR-142a inhibitor, miR-142a-3p knockdown group. Data are presented as the mean ± SEM. *$p < 0.05$; **$p < 0.01$.

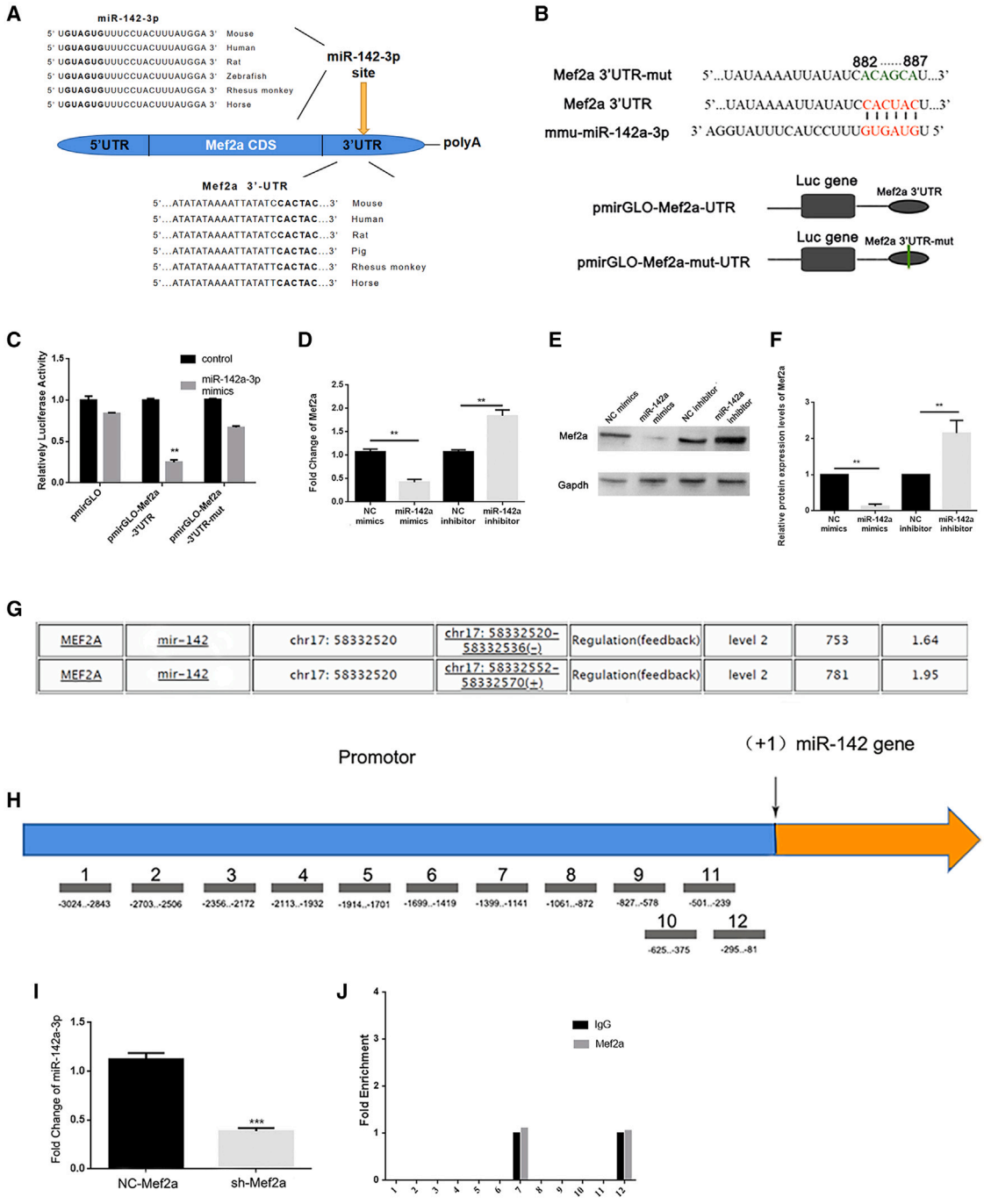

Figure 2. MiR-142a-3p targets Mef2a in the 3' UTR

(A) Schematic diagram of the structural sequence of the Mef2a 3' UTR, Mef2a 3′ UTR mut, miR-142a, and luciferase reporter. (B) The luciferase reporter was transfected into HEK-293T cells with the miR-142a mimic or control, and the luciferase activity was measured 24 h after transfection. (C–E) qRT-PCR and western blot analysis showed that miR-142a-3p inhibits the expression of Mef2a at the mRNA and protein levels (n = 3 per group). (F) TransmiR v2.0 predicted the binding site of Mef2a protein and miR-142a-3p promoter region. (G) Allocation of 12 primers of miR-142 promoter. (H) In Mef2a-knockdown C2C12 cells, miR-142a-3p expression decreased. (I) ChIP analysis of Mef2a at 12 positions of miR-142 promoter in C2C12. NC mimics, overexpression control group; MiR-142a mimics, miR-142a-3p overexpression group; NC inhibitor, knockdown control group; MiR-142a inhibitor, miR-142a-3p knockdown group. Data are presented as the mean ± SEM. *$p < 0.05$; **$p < 0.01$.

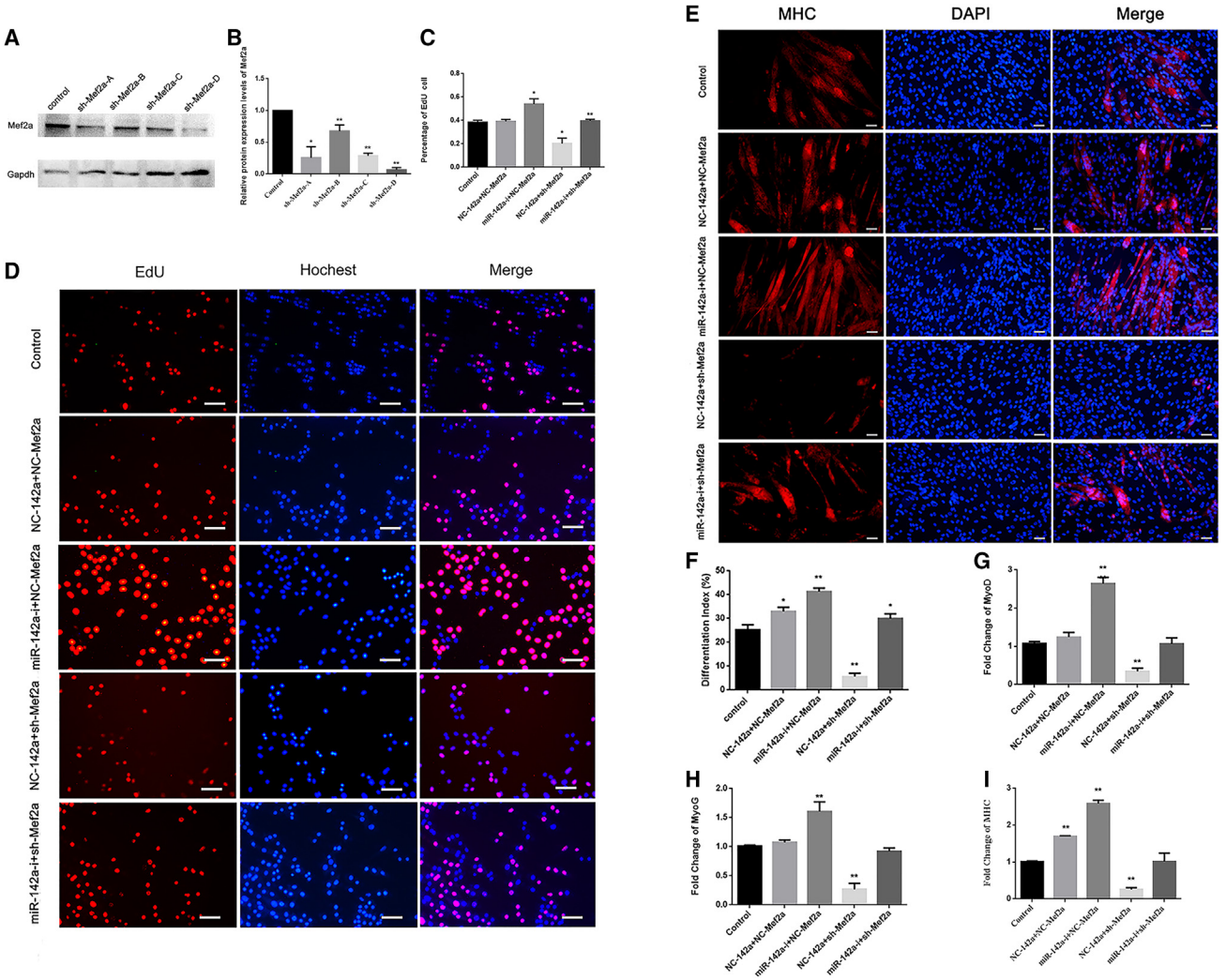

Figure 3. MiR-142a-3p inhibits C2C12 proliferation and differentiation by targeting Mef2a

(A and B) Western blot analysis showed that the D sequence had the highest knockdown efficiency. (C and D) EdU staining showed that knocking down Mef2a attenuated the effect of knocking down miR-142a-3p on cell proliferation promotion. (E and F) Immunofluorescence staining and differentiation index per field showed that knocking down Mef2a can attenuate the effect of knocking down miR-142a-3p on cell differentiation promotion. Muscle bundles were stained red by an anti-MHC antibody, and cell nuclei were stained blue by DAPI. (G–I) qRT-PCR analysis showed that knocking down Mef2a attenuated the effect of knocking down miR-142a-3p on the promotion of MyoG, MyoD, and MHC expression (n = 3 per group; scale bar, 500 μm for C and 50 μm for D). Control group, virus-free control group; NC-142a, miR-142a-3p knockdown control; NC-Mef2a, Mef2a knockdown control; MiR-142a-i, miR-142a-3p knockdown; Sh-Mef2a, Mef2a knockdown. Data are presented as the mean ± SEM. *$p < 0.05$; **$p < 0.01$.

control + Mef2a knockdown group, and miR-142 knockdown + Mef2a knockdown group. The right sciatic nerve of the mice in each group was clamped, and the distal sciatic nerve on the clamped side was harvested 2 weeks later, and immunofluorescence staining was performed after cross-section. As shown in Figures 4E and 4F, Schwann cells are marked in red, axons are marked in green, and nuclei are marked in blue. There was no significant difference in the number of regenerated axons among the groups, suggesting a consistent degree of nerve injury. Based on this, subsequent experiments to detect the degree of muscle atrophy can indicate the influence of miR-142a-3p on muscle.

MiR-142a-3p knockdown can relieve muscle atrophy after nerve clamp injury

2 weeks after the clamp injury, the muscle strength of the right tibial anterior muscle was measured. Compared with that of the control group, the muscle strength of the miR-142a-3p knockdown group was significantly greater, that of the Mef2a knockdown group was lower, and that of the co-knockdown group was in the middle (Figures 5A and 5B). In addition, through morphological observation, wet muscle weighing, and hematoxylin and eosin (H&E) staining (myotube diameter), it was found that miR-142a-3p knockdown significantly relieved the decrease in wet weight and myotube diameter after

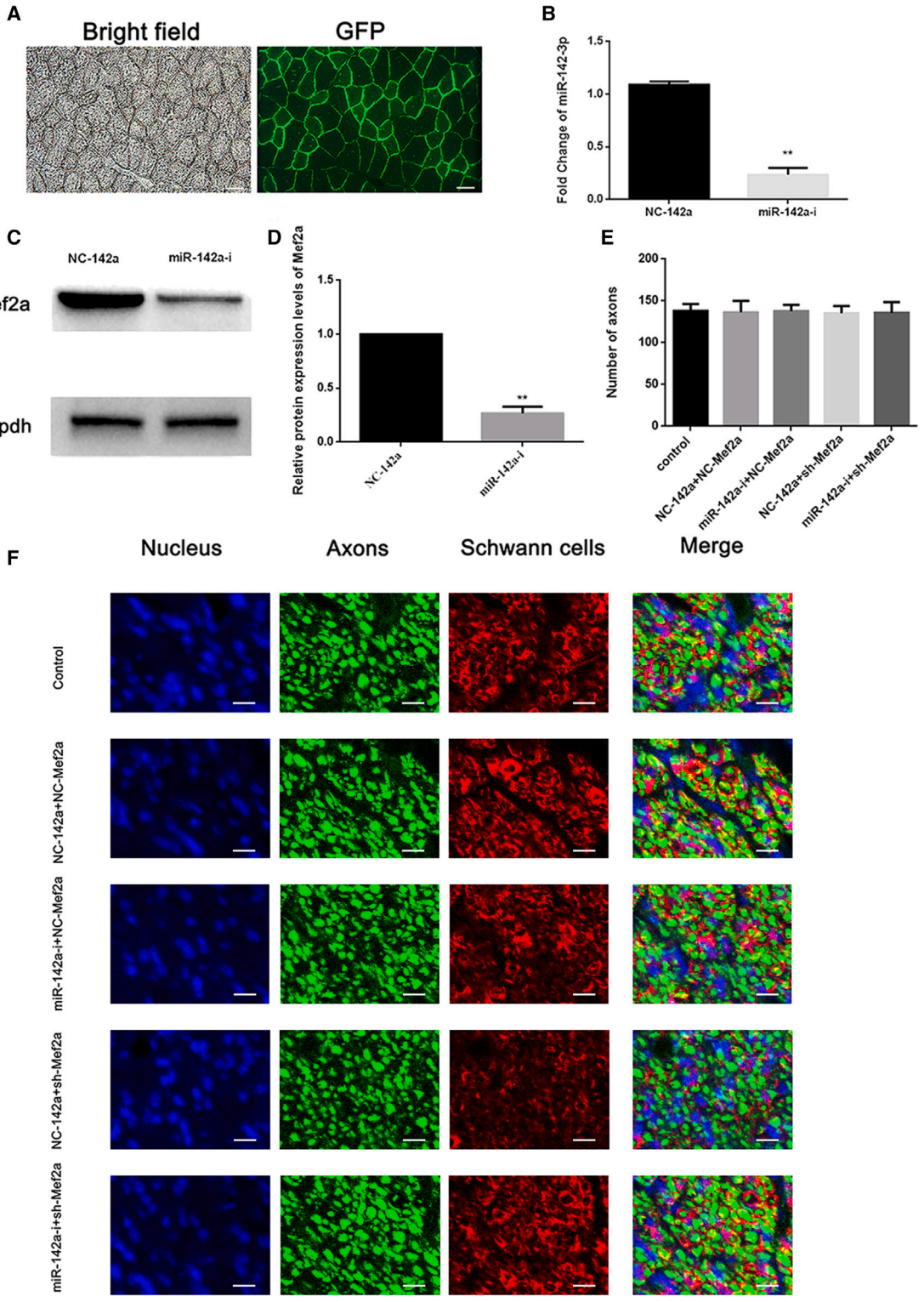

(legend on next page)

nerve clamping. This effect of miR-142a-3p knockdown was mitigated or offset by Mef2a knockdown (Figures 5C–5G) (Table 1). After muscle injury, satellite cells are activated to proliferate and eventually differentiate, allowing damaged muscle to regenerate. Therefore, we detected the number of satellite cells in the cross-section of skeletal muscle on the injured side in each group. Pax7 is a representative marker of proliferating muscle satellite cells, and immunofluorescence staining of Pax7-positive cells indicates proliferating satellite cells. The results showed that miR-142a-3p knockdown increased the number of proliferating satellite cells (Figures 6A and 6B). qRT-PCR was used to detect the expression of key genes in the injured side (R) and the healthy side (L). We detected the expression of the proliferation-related genes cdkn1a (p21), Cyclin B, Cyclin D, and Cyclin E; the muscle atrophy-related genes Atrogin-1, Murf-1 (Trim63), Nedd4, and Fbxo40; and the differentiation-related genes Myod, Myog, and MHC. The results showed that miR-142a-3p knockdown increased p21 and Myog expression and decreased Atrogin-1, Murf-1, and Nedd4 expression compared with that of the healthy side and the other groups, and Mef2a knockdown had the opposite effect (Figures 6C–6E).

DISCUSSION

The pathological process of neurogenic muscle atrophy involves a complex regulatory network, among which the most important factors include the depletion of muscle satellite cells (MSCs), the functional status of myoblasts, and changes in related protein metabolism and enzyme activity. This study attempted to explore the effect of miR-142a-3p/Mef2a axis on the pathological process of denervation muscular atrophy and its relationship with the main factors affecting muscle atrophy.

In vitro, the dual luciferase assay results confirmed that miR-142a-3p directly targeted Mef2a via complementary base pairing and inhibited its expression. Immunoprecipitation results showed that Mef2a did not regulate the expression of miR-142a-3p as a transcription factor. The miR-142a-3p/Mef2a axis effectively regulated the proliferation and differentiation of C2C12 myoblasts and affected the expression of MyoG, MyoD, and MHC, the key factors of muscle fusion. In this part of the study, we used C2C12 cells, which were established by Yaffe et al.[14] and can differentiate to form myoblasts capable of contraction under low-serum-induced conditions and can express various marker proteins of mature skeletal muscle such as myosin and myogenin.[15] Therefore, C2C12 cells are often the preferred model for studying myogenic cell proliferation and differentiation *in vitro*. The dual luciferase assay was validated on 293T cells rather than muscle cells, providing indirect evidence. Knockdown of Mef2a resulted in down-regulation of miR-142a-3p, but co-immunoprecipitation was negative, suggesting that Mef2a may affect the expression of miR-142a-3p through other indirect means but not as a transcription factor. In addition, the differentiation index of C2C12 in this study was about 25%, and that index was 20%–40% in most relevant studies, which may be related to cell inoculation density and differentiation time.[16–18]

In vivo, miR-142a-3p knockdown alleviated the decline in muscle strength, weight, and muscle fiber cross-sectional area caused by nerve clamp injury. miR-142a-3p knockdown also led to an increase in the number of MSCs and changes in the expression of genes related to proliferation, differentiation, and muscle atrophy, which could be alleviated or offset by Mef2a inhibition. In this part of the study, the sciatic nerve was pinched with a clamp, and the nerve at the injured site was stained 2 weeks later. Similar nerve regeneration was observed in each group, indicating that the degree of injury was homogeneous. At the same time, tibialis anterior muscle was taken, the transfection efficiency of AAV was confirmed under fluorescence microscope, and the gene knockdown was confirmed by PCR and western blot. In addition, 2 weeks after clamp injury is a significant period of pathological changes in skeletal muscle; it is representative to observe gene knockout effects at this time.

In vivo and *in vitro*, the miR-142a-3p/Mef2a axis has been found to play a role in denervated muscle atrophy and has contributed to several factors affecting muscle atrophy. First, miR-142a-3p regulated the proliferation and differentiation of C2C12 myoblasts, which is essential for the repair of injured skeletal muscle.[19–21] Previous studies have shown that some miRNAs have opposing roles in proliferation and differentiation, such as miR-22 inhibiting C2C12 proliferation and promoting differentiation.[22] There are also some miRNAs that have the same role in proliferation and differentiation, such as miR-203 and miR-696.[23,24] Overexpression of miR-142a-3p arrests more cells in the G0/G1 phase and inhibits their entry into differentiation. Mechanically, increased Myog expression signifies preparation for differentiation; then, the cells begin to express p21 and irreversibly exit the cell cycle; after that, myoblasts begin to differentiate and express MHC; finally, MHC-positive myoblasts fuse into myotubes.[25,26] In addition, the MyoD family regulates muscle differentiation and maturation,[27–29] and these proteins also direct the activation and differentiation of MSCs.[30] The above suggests that miR-142a-3p knockdown may cause muscle cells to exit the cell cycle by increasing p21 in skeletal muscle and increasing the expression of MyoG, MyoD, and MHC to promote cell fusion and ultimately repair muscle.

Second, miR-142a-3p knockdown promoted the proliferation of MSCs. Under normal physiological conditions, SCs of adult skeletal muscle are in a quiescent state. After injury or muscle movement, they are regulated by MyoD and Myf5, and thus activated, they begin

Figure 4. Establishment of the animal model

(A) 1 week after injection, the expression level of GFP-tagged protein was observed under a fluorescence microscope. (B) qRT-PCR showed that the miR-142a-3p knockdown rate exceeded 70%. (C and D) Western blot analysis showed that the Mef2a knockdown rate exceeded 70%. (E and F) Immunofluorescence image of the distal sciatic nerve after clamp injury (transverse section). Blue indicates nuclei, green indicates axons, and red indicates Schwann cells. (n = 6 per group; scale bar, 10 μm for F). Control group, PBS group; NC-142a, miR-142a-3p knockdown control; NC-Mef2a, Mef2a knockdown control; MiR-142a-i, miR-142a-3p knockdown; Sh-Mef2a, Mef2a knockdown. Data are presented as the mean ± SEM. *p < 0.05; **p < 0.01.

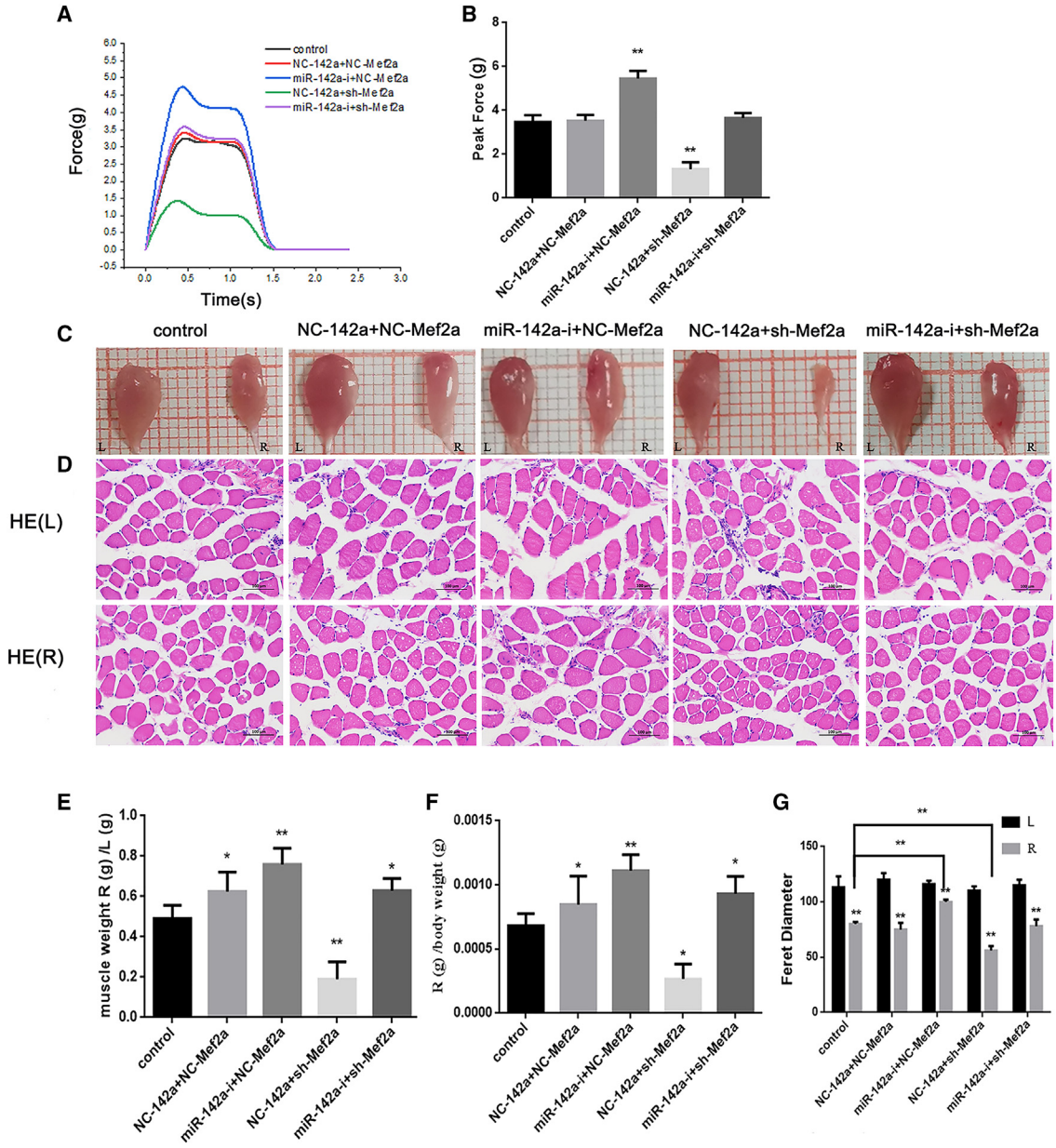

Figure 5. Knockdown of miR-142a-3p relieves tibialis anterior muscle atrophy after nerve clamp injury

(A and B) The results of muscle strength testing and peak muscle strength statistical analysis show that miR-142a-3p alleviates the weakening of muscle strength caused by neurogenic muscle atrophy. (C) Morphological observation of the injured side (R) and healthy side (L) tibialis anterior muscle of each group. (D) H&E staining was used to observe the cross-sections of myotubes. (E, F) Both the wet weight of the injured side/healthy side and the injured side body weight showed that the miR-142a-3p knockdown group retained greater muscle weight. (G) Statistical analysis of bilateral myotube Feret diameters in each group showed that the miR-142a-3p knockdown group retained larger fiber diameters (n = 6 per group; scale bar, 100 μm for D). Control group, PBS group; NC-142a, miR-142a-3p knockdown control; NC-Mef2a, Mef2a knockdown control; MiR-142a-i, miR-142a-3p knockdown; Sh-Mef2a, Mef2a knockdown; L, left; R, Right. Data are presented as the mean ± SEM. *$p < 0.05$; **$p < 0.01$.

to proliferate and eventually differentiate into fusion-competent myoblasts to regenerate damaged muscles.[20,31] Many ncRNAs have been found to regulate the functional state of MSCs.[32] MiR-142a-3p knockdown promoted the proliferation of MSCs, which may be one of the reasons why it alleviated neuromuscular atrophy.

Third, miR-142a-3p has a regulatory effect on the key proteins and enzymes of muscle atrophy. Activation of the ubiquitin-proteasome system is the main cause of muscle depletion,[33,34] and two muscle-specific ubiquitin ligases, Murf1 and Atrogin-1, are widely regarded as markers to accelerate the process of proteolysis

Table 1. The statistical data of the muscle weight

	Control	NC-142a+NC-Mef2a	miR-142a-i+NC-Mef2a	NC-142a+sh-Mef2a	miR-142a-i+sh-Mef2a
Muscle weight right/left	0.49 ± 0.03	0.63 ± 0.04	0.76 ± 0.03	0.19 ± 0.04	0.63 ± 0.02
Muscle weight right/body weight (%)	0.068 ± 0.0038	0.085 ± 0.0090	0.111 ± 0.0050	0.027 ± 0.0047	0.093 ± 0.0055

and atrophy.[35–37] Nedd4, compared with Murf1, shows a longer-lasting induction effect in denervated muscle.[38,39] MiR-142a-3p knockdown resulted in downregulation of Atrogin-1, Murf-1, and Nedd4, potentially inhibiting the activation of the ubiquitin-proteasome system and other muscle atrophy pathways. This may be one of the reasons that miR-142a-3p knockdown can alleviate denervated muscle atrophy.

The regulation of the above genes by miR-142a-3p can be attenuated or reversed by Mef2a. The mechanism by which the miR-142a-3p/Mef2a axis regulates the above genes is not very clear. On the one hand, miR-142a-3p may either directly target and regulate them at the gene level or indirectly target Mef2a. On the other hand, Mef2a may regulate downstream genes by influencing their transcription as a transcription factor or by PPIs. Currently, it is known that the MyoD family and Mef2 factors interact with each other at the protein level to control skeletal muscle mass.[40] In addition, Mef2a has been shown to regulate the transcription of many genes associated with skeletal muscle regeneration and atrophy.[41,42] On this basis, we speculated on the possible functional mechanism of the miR-142a-3p/Mef2a axis (Figure 7).

Conclusions

The repair effects of miR-142a-3p on neuromuscular atrophy may include both inhibition of muscle atrophy and promotion of myogenesis through activation of MSCs and myoblast differentiation. These data suggest that inhibition of miR-142a-3p may represent a novel approach for the treatment of neuromuscular atrophy.

MATERIALS AND METHODS

Cell culture and differentiation

Dulbecco's modified Eagle's medium (DMEM) (D5523, Sigma, Missouri, USA) supplemented with 10% fetal bovine serum (SH30406.05, HyClone, Utah, USA) and 1% penicillin/streptomycin (15140163, Invitrogen, USA) was used to culture cells and was changed every 2 days. DMEM high-glucose medium supplemented with 2% horse serum (26050088, Gibco, USA) and 1% penicillin/streptomycin (15140163, Invitrogen, USA) was used to induce cell differentiation and was changed every 3 days.

qRT-PCR

Total RNA was extracted from cells with TRIzol (15596026, Invitrogen, USA). Specific reverse transcription and q-PCR of miRNAs was initiated using specific stem-loop primers with Bulge-LoopTM miRNA qRT-PCR Kit (C10211-3, RiboBio, Guangzhou, China). The q-PCR primers are shown in Table S3.

Western blotting

Total protein isolations from C2C12 cells were prepared by standard procedures and assessed by the Pierce Micro BCA Protein Assay Kit (23235, Thermo Fisher, USA). 100 μg of protein per sample was separated on an 8% separation gel, and a 5% concentrated gel was used for sodium dodecyl sulfate/polyacrylamide gradient gel electrophoresis, followed by transfer onto Immun-Blot polyvinylidene fluoride membranes (IPVH00010, Millipore, USA) using a BIO-RAD Mini protein tetra system. All antibodies used were commercial antibodies, including goat anti-rabbit IgG H&L (HRP) (ab6721, Abcam, UK), rabbit anti-mouse IgG H&L (HRP) (ab6728, Abcam, UK), anti-beta actin (ab8226, Abcam, UK), and anti-MHC (M4276, Sigma, USA). Immunoreactivity was detected with Immobilon Western Chemiluminescent HRP-DAB substrate (Tiangen, Beijing, China).

RNA oligonucleotides and cell transfection

In this experiment, lentiviral transfection was used to achieve gene overexpression and knockdown. The vectors of miR-142a-3p mimic, negative control (NC) mimic,miR-142a-3p inhibitor, and NC inhibitor were purchased from Shanghai Genechem, and miR-142a-3p inhibitor was an antisense microRNA sequence, which competitively binds mature microRNA in cells, thereby affecting the binding of mature microRNA and target genes and reducing the inhibition of the microRNA on mRNA translation of target genes. Mef2a Mouse shRNA Plasmid and NC Plasmid were purchased from ORIGENE (TL501328, ORIGENE, Maryland, USA). The vectors were constructed and packaged by lentivirus for cell experiments.

The cells were seeded at 1×10^5 to 5×10^5 per well in a 24-well culture plate containing appropriate growth medium, and transfection was started when the cell density reached 30%–50%. The lentivirus was diluted to 1.5×10^7 TU/ml, and polybrene was diluted to 50 μg/mL, the medium in each well was washed away, and the medium, polybrene, and lentivirus were sequentially added. The culture plate was incubated in a 5% CO_2 incubator at 37°C for 72 h and observed by a fluorescence microscope. An infection rate of 80% or more was used for the experiment.

EdU assays

EdU assays were performed using an EdU assay kit (C10310–2, RiboBio, Guangzhou, China) according to the manufacturer's instructions. Briefly, 24 or 36 h after transfection, cells were exposed to 50 mM EdU for 3 h. Next, the cells were fixed with 4% paraformaldehyde (P0099, Beyotime, China) and permeabilized with 0.5% Triton X-100 (1.08643.6025, Merck Millipore, USA). Subsequently, the cells were

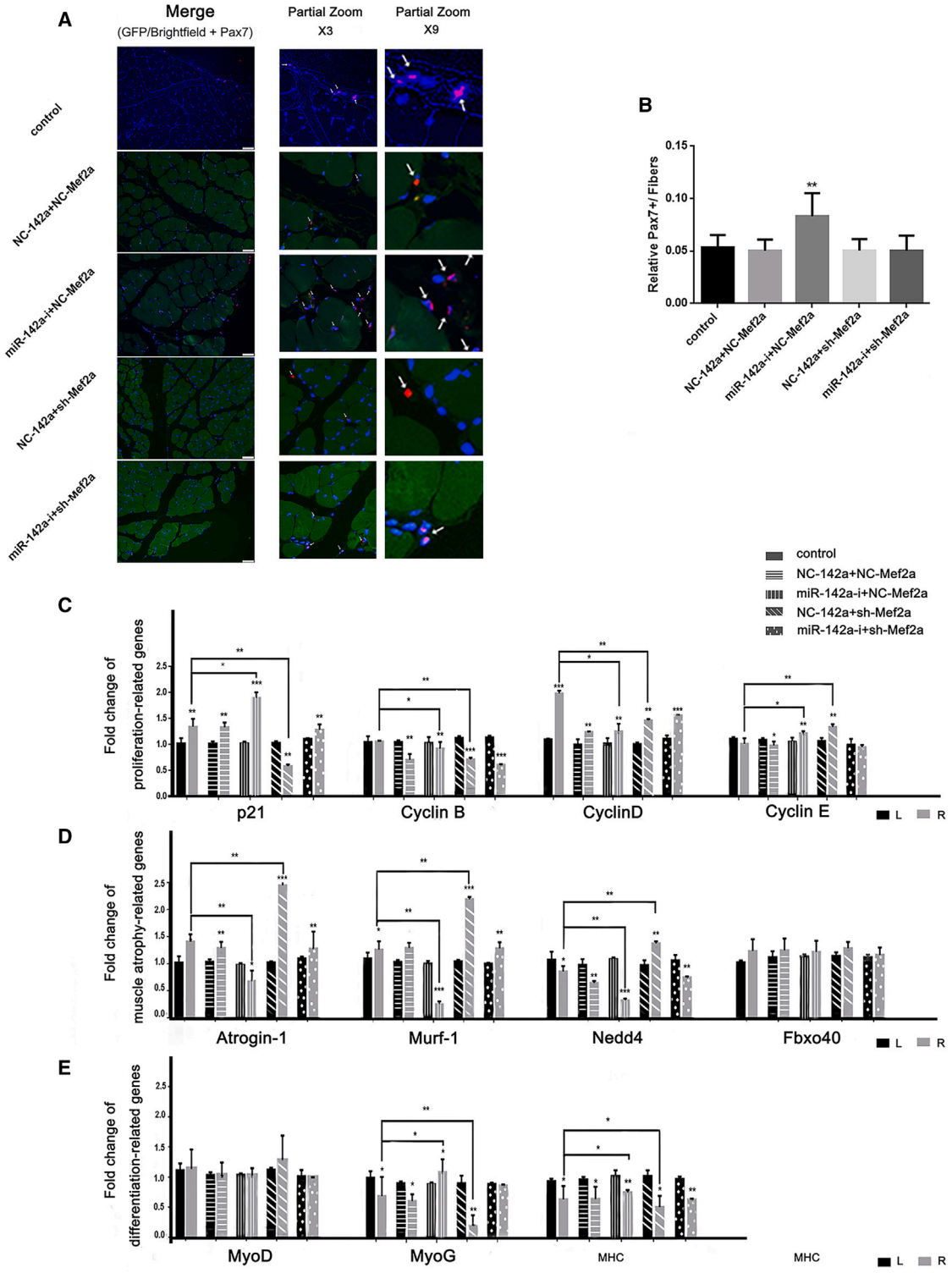

(legend on next page)

incubated in Apollo reaction solution for 1 h and stained with Hoechst 33342 for 30 min. The cells were further analyzed by calculating the ratio of EdU-positive cells to the total number of cells.

Cell cycle flow cytometry

All steps were followed in the instructions of the Cell Cycle and Apoptosis Analysis Kit (C1052, Beyotime, China). After transfection for 24 or 36 h, cells were fixed in 70% (v/v) ethanol (E111963, Aladdin, China) overnight at −20°C. Following incubation in 50 mg/mL propidium iodide (provided by kit) with 100 mg/mL RNase A (provided by kit) and 0.2% (v/v) Triton X-100 (1.08643.6025, Merck Millipore, USA) for 30 min at 4°C, the cells were analyzed in a FACSCalibur flow cytometer (BD Biosciences) and with ModFit software.

Dual luciferase reporter assays

293T cells were cotransfected with 100 ng of wild-type or mutant 3′ UTR luciferase reporter and 40 nM miR-142a mimics or NC mimics using X-tremegene HP (06366236001, ROCHE, Switzerland) in 24-well plates. After transfection for 24 h, the activities of firefly and Renilla luciferase were measured using a dual luciferase reporter assay system (E1910, Promega, USA) following the manufacturer's instructions. The Renilla luciferase signal was normalized to the firefly luciferase signal.

Chromatin immunoprecipitation (ChIP) assay

The ChIP-IT High Sensitivity kit (53040, Active Motif, USA) was used for the ChIP experiment. 10^7 C2C12 cells were used for the experiment. All steps were carried out according to the instructions. The final sample was incubated with anti-Mef2a (PA5-27380, Invitrogen, USA) or IgG (ab171870, Abcam, UK). PCR was performed after DNA was isolated from the immunoprecipitates. The q-PCR primers are shown in Table S4.

Animals

Male specific-pathogen-free (SPF)-grade C57BL/6 mice, 6–8 weeks old and weighing 22–25 g, were purchased from Beijing Vital River Laboratory Animal Technology (Beijing, China) and raised in the Animal Experiment Center of Peking University People's Hospital. The animals were kept in separate cages and were free to drink and eat, the room temperature was controlled at 21°C–23°C, and the day and night cycle light was 12 h/12 h. The animal protection regulations of Peking University Health Science Center were strictly followed, and all laboratory animal operations were approved by the Animal Ethics Review Committee of Peking University People's Hospital and complied with laboratory animal ethics policies and regulations (ethics approval number: 2017PHC004).

Immunofluorescence

Cells treated in six-well plates were fixed in 4% formaldehyde (P0099, Beyotime, China) for 20 min and then washed three times for 5 min each time with PBS (P-1020, Solarbio, China). The cells were then permeabilized with 0.1% Triton X-100 (1.08643.6025, Merck Millipore, USA) for 15 min. The cells were incubated in blocking solution (SL1336, Coolaber, China) for 1 h at room temperature. After blocking, the cells were incubated with an anti-MHC antibody (M4276, Sigma, USA, 1:500) overnight at 4°C. The next day, a secondary Alexa Fluor 594 goat anti-mouse IgG antibody (ab150116, Abcam, UK) was incubated with the samples for 2 h at room temperature. The cell nuclei were visualized with DAPI staining (236276, Whatman, UK).

Adeno-associated virus injections in mice

The vectors of miR-142a-3p inhibitor, NC inhibitor, Mef2a Mouse shRNA Plasmid, and NC Plasmid were purchased from Shanghai Genechem. The vector was constructed and packaged by AAV for *in vivo* experiments. The AAV particles (Genechem, China) used for gene knockdown were injected into the right tibialis anterior muscle of mice at a dose of 10.0×10^{11} IU/mL. The multipoint injection method was used, with one needle each in the upper, middle, and lower parts of the muscle and 5 μL per needle. A total of 15 μL of virus preparation was injected into each muscle. The control group was injected with PBS (P-1020, Solarbio, China) in the same manner and dose.

PNI model establishment

Mice were anesthetized by intraperitoneal injection with 1% ketamine (8 mg/100 g of body weight), followed by shearing and disinfection of the skin prior to surgery. The sciatic nerve of the right leg was exposed and clamped for 30 s each using 2-mm-wide pincers (Shanghai Medical Devices, Shanghai, China). The location of the distal portion of the injured nerve was marked by a 10-0 nylon microscopic suture. The incision was then closed. All operations were performed on the right hindlimb, while the left hindlimb served as the nonoperated control.

Staining

Gastrocnemius muscle samples were freshly separated and mounted in 4% paraformaldehyde (P0099, Beyotime, China). The muscle was cut into 10-μm-thick sections for H&E staining and periodic acid-Schiff staining. The H&E staining kit (C0105, Beyotime, China) and Periodic Acid-Schiff Stain Kit (C0142, Beyotime, China) were used. The staining steps were carried out in accordance with the instructions.

To identify MSCs, muscle paraffin sections were gradually deparaffinized with xylene, put into distilled water, and then put into heated antigen retrieval solution. Antigen retrieval was performed in a pressure cooker for 10 min. After antigen retrieval, the sections were washed

Figure 6. MiR-142a-3p affects muscle satellite cells and muscle transcriptome expression

(A) Blue indicates nuclei, green indicates GFP-tagged protein (the control group image was replaced by a bright field image due to no injection of the virus), and red indicates Pax7+ cells. (B) Counting the number of Pax7+ cells/myotubes in each group showed that the miR-142a-3p knockdown group maintained more activated satellite cells. qRT-PCR was used to detect the expression of genes related to (C) proliferation, (D) muscle atrophy, and (E) muscle differentiation of the bilateral tibialis anterior muscles (n = 6 per group; scale bar, 50 μm). Control group, PBS group; NC-142a, miR-142a-3p knockdown control; NC-Mef2a, Mef2a knockdown control; MiR-142a-i, miR-142a-3p knockdown; Sh-Mef2a, Mef2a knockdown; L, left; R, Right. Data are presented as the mean ± SEM. *$p < 0.05$; **$p < 0.01$.

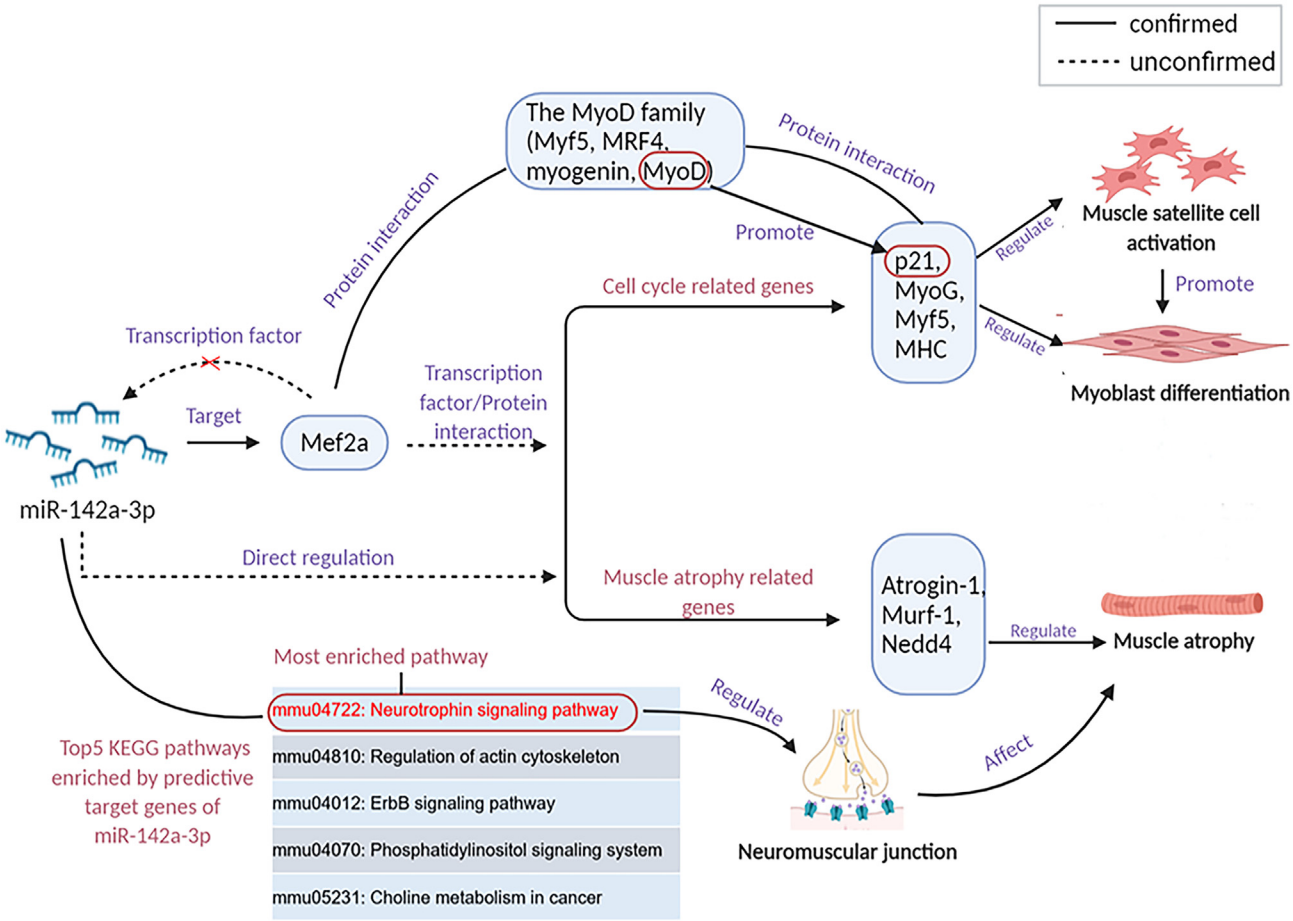

Figure 7. Hypothesis regarding the miR-142a-3p/Mef2a axis mechanism of regulation of neurogenic skeletal muscle atrophy
The figure was drawn using BioRender website (https://app.biorender.com/gallery).

with PBS (P-1020, Solarbio, China), placed in a wet box, soaked with immunofluorescence blocking solution, and incubated for 1 h at room temperature. Muscle was incubated overnight at 4°C with an anti-Pax7 antibody (ab187339, Abcam, UK, 1:100) diluted in 5% BSA. Then, muscle was incubated with the Goat Anti-Rabbit IgG H&L (Alexa Fluor 555) (ab150078, Abcam, UK, 1:500) for 1 h at room temperature. Nuclear staining was performed with DAPI (236276, Whatman, UK). Images were captured by fluorescence microscopy (Leica).

To analyze the regenerated axons, the sciatic nerve was incubated overnight in 4% paraformaldehyde (P0099, Beyotime, China) and cross-sectioned into frozen sections with a thickness of 8 μm. Finally, immunofluorescence staining was performed: axons, NF200 (N0142, Sigma, USA); Schwann cells, S-100 (ab52642, Abcam, UK); and nuclei, DAPI (236276, Whatman, UK). Images were captured by a TCS-SP8 DIVE confocal laser microscope (Leica).

In situ muscle functional testing

The tibialis anterior muscle was separated, the adjacent joints were fixed on a special fixation frame, and the distal tendons were cross-sutured with silk threads and connected to the traction receptors (MLT500/D, Force Transducer, ADInstruments) so that the direction of the muscle and the receptors was maintained in the same straight line. The traction tension was adjusted to maintain a certain degree of initial load ($0 < F < 0.1$ N). A stimulating electrode was placed on the sciatic nerve, and continuous electrical stimulation was given at 0.9 mA, a wave width of 0.1 ms, and a frequency of 50 Hz. The waveform of the tonic contraction force was recorded.

Statistical analysis

Prism v8.2.1 and OriginPro 2019 were used for data analysis and graphing. Student's t test was used to analyze the data, and all values are expressed as the mean ± SEM. Differences were considered significant with $p < 0.05$.

DATA AVAILABILITY

The authors confirm that the data supporting the findings of this study are available within the article and its supplemental information.

SUPPLEMENTAL INFORMATION

Supplemental information can be found online at https://doi.org/10.1016/j.omtn.2023.05.023.

ACKNOWLEDGMENTS

This work was supported by the grants from National Natural Science Foundation of China (82072162 to X.Y. and 81971177 to B.J.) and Natural Science Foundation of Beijing, China (7192215 to X.Y.).

AUTHOR CONTRIBUTIONS

X.Y. designed the study. X.G. instructed all experiments and drafted the manuscript. S.W., D.L., B.J., Z.Q., J.D., and C.H. analyzed the data.

DECLARATION OF INTERESTS

The authors declare no competing financial interests.

REFERENCES

1. Özaksar, K., Günay, H., Küçük, L., and Coşkunol, E. (2017). Long-term results of primary repair of combined cuts on the median and ulnar nerves in the forearm. Ulus Travma Acil Cerrahi Derg *23*, 410–414.
2. Viguie, C.A., Lu, D.X., Huang, S.K., Rengen, H., and Carlson, B.M. (1997). Quantitative study of the effects of long-term denervation on the extensor digitorum longus muscle of the rat. Anat. Rec. *248*, 346–354.
3. Chen, J.F., Mandel, E.M., Thomson, J.M., Wu, Q., Callis, T.E., Hammond, S.M., Conlon, F.L., and Wang, D.Z. (2006). The role of microRNA-1 and microRNA-133 in skeletal muscle proliferation and differentiation. Nat. Genet. *38*, 228–233.
4. Liu, N., Williams, A.H., Maxeiner, J.M., Bezprozvannaya, S., Shelton, J.M., Richardson, J.A., Bassel-Duby, R., and Olson, E.N. (2012). microRNA-206 promotes skeletal muscle regeneration and delays progression of Duchenne muscular dystrophy in mice. J. Clin. Invest. *122*, 2054–2065.
5. Weng, J., Zhang, P., Yin, X., and Jiang, B. (2018). The whole transcriptome involved in denervated muscle atrophy following peripheral nerve injury. Front. Mol. Neurosci. *11*, 69.
6. Fiorillo, A.A., Tully, C.B., Damsker, J.M., Nagaraju, K., Hoffman, E.P., and Heier, C.R. (2018). Muscle miRNAome shows suppression of chronic inflammatory miRNAs with both prednisone and vamorolone. Physiol. Genom. *50*, 735–745.
7. Kinder, T.B., Heier, C.R., Tully, C.B., Van der Muelen, J.H., Hoffman, E.P., Nagaraju, K., and Fiorillo, A.A. (2020). Muscle weakness in myositis: MicroRNA-mediated dystrophin reduction in a myositis mouse model and human muscle biopsies. Arthritis Rheumatol. *72*, 1170–1183.
8. Gu, X.Y., Jin, B., Qi, Z.D., and Yin, X.F. (2022). MicroRNA is a potential target for therapies to improve the physiological function of skeletal muscle after trauma. Neural Regen. Res. *17*, 1617–1622.
9. Chemello, F., Grespi, F., Zulian, A., Cancellara, P., Hebert-Chatelain, E., Martini, P., Bean, C., Alessio, E., Buson, L., Bazzega, M., et al. (2019). Transcriptomic analysis of single isolated myofibers identifies miR-27a-3p and miR-142-3p as regulators of metabolism in skeletal muscle. Cell Rep. *26*, 3784–3797.e8.
10. Liu, B.L., Cheng, M., Hu, S., Wang, S., Wang, L., Tu, X., Huang, C.X., Jiang, H., and Wu, G. (2018). Overexpression of miR-142-3p improves mitochondrial function in cardiac hypertrophy. Biomed. Pharmacother. *108*, 1347–1356.
11. Gu, X., Jin, B., Qi, Z., and Yin, X. (2021). Identification of potential microRNAs and KEGG pathways in denervation muscle atrophy based on meta-analysis. Sci. Rep. *11*, 13560.
12. Taylor, M.V., and Hughes, S.M. (2017). Mef2 and the skeletal muscle differentiation program. Semin. Cell Dev. Biol. *72*, 33–44.
13. Kaushal, S., Schneider, J.W., Nadal-Ginard, B., and Mahdavi, V. (1994). Activation of the myogenic lineage by MEF2A, a factor that induces and cooperates with MyoD. Science *266*, 1236–1240.
14. Yaffe, D., and Saxel, O. (1977). Serial passaging and differentiation of myogenic cells isolated from dystrophic mouse muscle. Nature *270*, 725–727.
15. Niu, W., Bilan, P.J., Ishikura, S., Schertzer, J.D., Contreras-Ferrat, A., Fu, Z., Liu, J., Boguslavsky, S., Foley, K.P., Liu, Z., et al. (2010). Contraction-related stimuli regulate GLUT4 traffic in C2C12-GLUT4myc skeletal muscle cells. Am. J. Physiol. Endocrinol. Metab. *298*, E1058–E1071.
16. Osana, S., Kitajima, Y., Suzuki, N., Nunomiya, A., Takada, H., Kubota, T., Murayama, K., and Nagatomi, R. (2021). Puromycin-sensitive aminopeptidase is required for C2C12 myoblast proliferation and differentiation. J. Cell. Physiol. *236*, 5293–5305.
17. Yao, X., Yu, T., Zhao, C., Li, Y., Peng, Y., Xi, F., and Yang, G. (2018). Evodiamine promotes differentiation and inhibits proliferation of C2C12 muscle cells. Int. J. Mol. Med. *41*, 1627–1634.
18. Aley, P.K., Mikolajczyk, A.M., Munz, B., Churchill, G.C., Galione, A., and Berger, F. (2010). Nicotinic acid adenine dinucleotide phosphate regulates skeletal muscle differentiation via action at two-pore channels. Proc. Natl. Acad. Sci. USA *107*, 19927–19932.
19. Dumont, N.A., Bentzinger, C.F., Sincennes, M.C., and Rudnicki, M.A. (2015). Satellite cells and skeletal muscle regeneration. Compr. Physiol. *5*, 1027–1059.
20. Tedesco, F.S., Dellavalle, A., Diaz-Manera, J., Messina, G., and Cossu, G. (2010). Repairing skeletal muscle: regenerative potential of skeletal muscle stem cells. J. Clin. Invest. *120*, 11–19.
21. Schmidt, M., Schüler, S.C., Hüttner, S.S., von Eyss, B., and von Maltzahn, J. (2019). Adult stem cells at work: regenerating skeletal muscle. Cell. Mol. Life Sci. *76*, 2559–2570.
22. Wang, H., Zhang, Q., Wang, B., Wu, W., Wei, J., Li, P., and Huang, R. (2018). miR-22 regulates C2C12 myoblast proliferation and differentiation by targeting TGFBR1. Eur. J. Cell Biol. *97*, 257–268.
23. Luo, W., Wu, H., Ye, Y., Li, Z., Hao, S., Kong, L., Zheng, X., Lin, S., Nie, Q., and Zhang, X. (2014). The transient expression of miR-203 and its inhibiting effects on skeletal muscle cell proliferation and differentiation. Cell Death Dis. *5*, e1347.
24. Wang, H., Shi, L., Liang, T., Wang, B., Wu, W., Su, G., Wei, J., Li, P., and Huang, R. (2017). MiR-696 regulates C2C12 cell proliferation and differentiation by targeting CNTFRalpha. Int. J. Biol. Sci. *13*, 413–425.
25. Andrés, V., and Walsh, K. (1996). Myogenin expression, cell cycle withdrawal, and phenotypic differentiation are temporally separable events that precede cell fusion upon myogenesis. J. Cell Biol. *132*, 657–666.
26. Walsh, K., and Perlman, H. (1997). Cell cycle exit upon myogenic differentiation. Curr. Opin. Genet. Dev. *7*, 597–602.
27. Bar-Nur, O., Gerli, M.F.M., Di Stefano, B., Almada, A.E., Galvin, A., Coffey, A., Huebner, A.J., Feige, P., Verheul, C., Cheung, P., et al. (2018). Direct reprogramming of mouse fibroblasts into functional skeletal muscle progenitors. Stem Cell Rep. *10*, 1505–1521.
28. Conerly, M.L., Yao, Z., Zhong, J.W., Groudine, M., and Tapscott, S.J. (2016). Distinct activities of Myf5 and MyoD indicate separate roles in skeletal muscle lineage specification and differentiation. Dev. Cell *36*, 375–385.
29. Yamamoto, M., Legendre, N.P., Biswas, A.A., Lawton, A., Yamamoto, S., Tajbakhsh, S., Kardon, G., and Goldhamer, D.J. (2018). Loss of MyoD and Myf5 in skeletal muscle stem cells results in altered myogenic programming and failed regeneration. Stem Cell Rep. *10*, 956–969.
30. Zammit, P.S. (2017). Function of the myogenic regulatory factors Myf5, MyoD, Myogenin and MRF4 in skeletal muscle, satellite cells and regenerative myogenesis. Semin. Cell Dev. Biol. *72*, 19–32.
31. Gayraud-Morel, B., Chrétien, F., Flamant, P., Gomès, D., Zammit, P.S., and Tajbakhsh, S. (2007). A role for the myogenic determination gene Myf5 in adult regenerative myogenesis. Dev. Biol. *312*, 13–28.
32. Zhao, Y., Chen, M., Lian, D., Li, Y., Li, Y., Wang, J., Deng, S., Yu, K., and Lian, Z. (2019). Non-coding RNA regulates the myogenesis of skeletal muscle satellite cells, injury repair and diseases. Cells *8*.
33. Bilodeau, P.A., Coyne, E.S., and Wing, S.S. (2016). The ubiquitin proteasome system in atrophying skeletal muscle: roles and regulation. Am. J. Physiol. Cell Physiol. *311*, C392–C403.
34. Wiles, B., Miao, M., Coyne, E., Larose, L., Cybulsky, A.V., and Wing, S.S. (2015). USP19 deubiquitinating enzyme inhibits muscle cell differentiation by suppressing unfolded-protein response signaling. Mol. Biol. Cell *26*, 913–923.

35. Bodine, S.C., Latres, E., Baumhueter, S., Lai, V.K., Nunez, L., Clarke, B.A., Poueymirou, W.T., Panaro, F.J., Na, E., Dharmarajan, K., et al. (2001). Identification of ubiquitin ligases required for skeletal muscle atrophy. Science *294*, 1704–1708.

36. Gomes, M.D., Lecker, S.H., Jagoe, R.T., Navon, A., and Goldberg, A.L. (2001). Atrogin-1, a muscle-specific F-box protein highly expressed during muscle atrophy. Proc. Natl. Acad. Sci. USA *98*, 14440–14445.

37. Bodine, S.C., and Baehr, L.M. (2014). Skeletal muscle atrophy and the E3 ubiquitin ligases MuRF1 and MAFbx/atrogin-1. Am. J. Physiol. Endocrinol. Metab. *307*, E469–E484.

38. Batt, J., Bain, J., Goncalves, J., Michalski, B., Plant, P., Fahnestock, M., and Woodgett, J. (2006). Differential gene expression profiling of short and long term denervated muscle. Faseb. J. *20*, 115–117.

39. D'Cruz, R., Plant, P.J., Pablo, L.A., Lin, S., Chackowicz, J., Correa, J., Bain, J., and Batt, J. (2016). PDLIM7 is a novel target of the ubiquitin ligase Nedd4-1 in skeletal muscle. Biochem. J. *473*, 267–276.

40. Schiaffino, S., Dyar, K.A., and Calabria, E. (2018). Skeletal muscle mass is controlled by the MRF4-MEF2 axis. Curr. Opin. Clin. Nutr. Metab. Care *21*, 164–167.

41. Paris, J., Virtanen, C., Lu, Z., and Takahashi, M. (2004). Identification of MEF2-regulated genes during muscle differentiation. Physiol. Genom. *20*, 143–151.

42. Huang, H.T., Brand, O.M., Mathew, M., Ignatiou, C., Ewen, E.P., McCalmon, S.A., and Naya, F.J. (2006). Myomaxin is a novel transcriptional target of MEF2A that encodes a Xin-related alpha-actinin-interacting protein. J. Biol. Chem. *281*, 39370–39379.